공학석사학위논문

고층빌딩 곤돌라 탑재용 외부 유리창 청소로봇 유닛 개발

Development of gondola platform wall cleaning robot unit for high-rise building

2019 년 2 월

서울대학교 대학원

기계항공공학부

주 인 호

Abstract

Development of gondola platform wall cleaning robot unit for high-rise building

Inho Joo

Department of Mechanical and Aerospace Engineering

Seoul National University

Walls of high-rise buildings are cleaned manually several times in a year by workers in a gondola. The cleaning work is difficult and extremely dangerous for human workers and there are several ongoing studies to automate this work by means of robotic solutions. To achieve a successful cleaning performance, a cleaning operation has to adapt to the environmental conditions. In this study, we design and assemble a manipulator to be used in wall-cleaning applications. From the design requirements identified by investigating a high-rise building in Korea, we determined the two important degrees-of-freedom (DOF), and a parallel mechanism is designed to achieve the motion. With the parallel configuration, the design parameters are optimized based on a dynamic index to achieve high cleaning performance in a gondola. A prototype is assembled, and the cleaning performance is verified on a test bench. A field test with the developed manipulator will be performed in the near future.

Keyword : wall-cleaning, parallel mechanism, optimal design, dynamic modeling

Student Number : 2017-22895

Contents

1. Introduction 1

2. Condition for wall-cleaning operation 4

2.1 63-story building and gondola specification 4

2.2 Cleaning operation and cleaning performace 4

2.3 Motion and constraints of the gondola motion 5

3. 2-DOF manipulator for cleaning operation 7

3.1 Kinematic configuration and modeling 7

3.2 Jacobian matrix 10

3.3 Dynamic analysis 11

3.4 Mass matrix of the manipulator 12

4. Optimal design 23

4.1 Dynamic manipulator isotropy index 23

4.2 Workspace constraints 25

4.3 Optimization problem definition 25

4.4 Optimal design result 25

5. Prototype and experiment 31

6. Conclusion 31

Reference 32

초록 34

List of Figures

[Figure 1] Photograph and modeling of a 63-story building in Korea……4

[Figure 2] Cleaning module for wall-cleaning manipulator robot…….5

[Figure 3] Motions and constraints of the gondola in a 63-story building…….6

[Figure 4] Kinematic configuration of the proposed 2-DOF parallel manipulator…8

[Figure 5] Configuration diagram of the parallel manipulator……9

[Figure 6] Constraints on the workspace for the optimal design…….....16

[Figure 7] Optimal design result……..20

[Figure 8] Dynamic manipulability ellipsoid for y_e, θ_e in target workspace……21

[Figure 9] Prototype design and photograph of the assembled prototype……22

[Figure 10] Workspace test of the cleaning unit manipulated by the developed 2-DOF manipulator……..23

[Figure 11] Load cell sensors measure the force input by the operation of the manipulator……..24

[Figure 12] Input force ellipsoid graph of optimized and non-optimized manipulator……..25

[Figure 13] Test bench for the cleaning experiment……26

[Figure 14] Cleaning operation on a test bench and cleaning results……..26

List of Tables

[Table 1] Optimization condition ……19

[Table 2] Optimized design parameters ……...21

* Contents in this thesis will be published in the international journal.

1. Introduction

As the number of high-rise buildings around the world increases, the cleaning of the exterior walls has become an important issue. As a result, the demand for wall cleaning of high-rise buildings is steadily increasing. Presently, a high-rise building is cleaned by cleaning workers with ropes or on-board a gondola. Owing to the dangers of this cleaning work, the mortality rate of workers cleaning the exterior walls of buildings has increased every year. Thus, there have been attempts to replace the exterior-wall cleaning workers with robots.

There are several commercial solutions of wall-cleaning robots in the market. Skypro and IPC Eagle are the most popular examples of commercial cleaning robots [1–2]. TITO 500, SIRIUSc, and CAFÉ have been studied to clean outer walls [3–5]. Sky Cleaner clean tasks have also been developed, in which water is sprayed [6]. The building facade maintenance robot (BFMR) sweeps a wall by using nozzle and squeeze [7]. However, up to now, these cleaning units have been designed in a relatively simple way. Most of them using only water spray with roller brush, or spray with squeeze. Without squeeze, the water will be spread out and there will be second-contamination. And without brush, adhered contaminants will not be removed perfectly. Our wall-cleaning robot has a system with nozzle, brush, squeeze and suction parts. It could perfectly clean the window whether it is severely contaminated.

In this research, we propose a new wall-cleaning robot equipped in a gondola. As many high-rise buildings have a gondola as a part of their emergency and

maintenance system (EMS), we consider that this gondola is particularly useful to clean walls. The cleaning robot has two important components: the cleaning unit and the device that can manipulate the unit. The manipulator has the especially important role of changing the position and orientation of the cleaning unit to compensate for the external disturbances. Without a manipulator, the cleaning unit cannot be used in its optimal condition, and the cleaning operation cannot be performed successfully.

We design a 2-DOF wall-cleaning parallel manipulator based on the design requirements investigated in a 63-story building in Korea, which can adjust the distance as well as the contact angle with a wall. The design can be easily customized according to the different glass sizes of buildings. The manipulator is attached to the gondola of the building, and it can manipulate the cleaning unit for wall cleaning in the presence of various disturbances. Parallel manipulators possess the advantage of high stiffness, low inertia, and large payload capacity. Furthermore, the actuators are mounted on the base, and thus, they are relatively easy to customize by simply changing the length and joint of the link. In order to ensure the manipulator's optimal performance when customizing it to various buildings, an optimal design of the kinematic parameters is required for the 2-DOF parallel mechanism.

There are many references on 'dynamics of parallel manipulator' and 'optimizing the design of robot manipulators'. Jun Wu studied and evaluated the dynamics of various parallel manipulators[8–11]. Liu and Wang [12] used the PRRRP 2-DOF parallel manipulator with global conditioning index (GCI), global velocity index (GVI), global payload index (GPI), and global stiffness index (GSI) and presented examples that the designer could optimize using the desired indexes appropriately. Liu et al. [13] proposed a symmetric parallel manipulator and performed a kinematic optimization through the global conditioning index (GCI). In dynamic optimization, Asada [14] proposed the generalized inertia ellipsoid (GIE) and a method to analyze

the dynamic behavior. Khatib et al. [15,16] decomposed the mass and inertia so that the ellipsoid is respectively isotropy. The dynamic capability equation (DCE) is proposed and optimized by unification of dynamic acceleration, velocity, and force in the worst case. While kinematics optimization and dynamics optimization are usually performed sequentially, Liu et al. [17] optimized a parallel mechanism using a condition number via the genetic and sequential quadratic programming algorithm. We consider that we have to optimize the design parameters based on a specific index that refers to the cleaning operation appropriately.

The objective of this research is to propose a manipulator for wall-cleaning operations and optimize its design parameters. The optimal design is performed based on dynamic manipulability isotropy, a reliable index to increase the cleaning performance by increasing the isotropy of inertia matrix. Based on the dynamic manipulability isotropy index, we optimized the kinematic parameters of the manipulator. Kinematic and dynamic analyses are performed to obtain the index and simulate the movement. The workspace is used as the constraint. A working prototype is developed and the experiments are performed on a test bench to validate the cleaning performance.

The rest of this paper is as follows. Section 2 describes the design requirements investigated from a 63-story building in Korea. Based on these requirements, we propose a 2-DOF parallel manipulator for the cleaning operation in Section 3. Kinematic and dynamic analyses are also performed. Section 4 presents the procedure and results of the optimal design on the kinematic parameters to maximize the dynamic manipulability isotropy. Section 5 presents the prototype assembly and test result. The concluding remarks are included in Section 6.

2. Condition for wall-cleaning operation

2.1. 63-story building and gondola specification

To design the configuration of the manipulator, the information of the environment is investigated. We selected a 63-story building in Korea as a target building for the application [18]. The building has 63 stories with a height of 274 m. Each story is covered with a glass panel outside, with a size of 1,500 × 1,850 mm2. A photograph with the detailed dimensions is included in Fig. 1.

A gondola is equipped in the 63-story building. The gondola is typically used for glass cleaning and maintenance tasks. Figure 1(c) shows the shape and dimensions of the gondola. The gondola is supported by four steel wires, and the winch for the wires is located on the ceiling. The width of the gondola is 7,000 mm, which can cover five glass panels in the lateral direction. By using the DOF of the gondola system, we do not need to develop a mobile device on the wall, and a simple manipulator can be equipped in the gondola to conduct the cleaning operation.

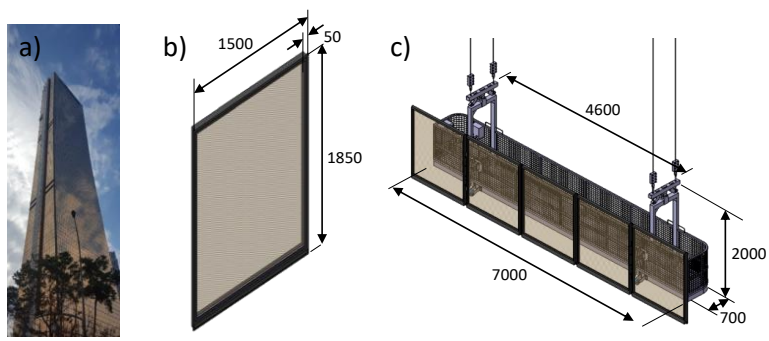

Fig. 1 Photograph and modeling of a 63-story building in Korea. a) overall shape of the 63-story building [18], b) dimensions of one glass panel, and c) gondola dimension with the glass panels.

2.2 Cleaning operation and cleaning performance

In Figure 2, the cleaning, which is attached on the end-effector of the wall-cleaning robot, consists of four parts [23]. This module cleans with nozzle, roller brush, squeeze and suction parts. As the gondola descends from the roof of the building, the cleaning module contacts to the window. The nozzle sprays the water to the window, and the roller brush rotates and sweeps contaminant which is attached on the window. The squeezes are placed at the upper side and lower side of the cleaning module. As the water and the contaminant flow down the surface of the window, the lower squeeze blocks the gap and gather them. And the upper squeeze wipes and gathers the water and the contaminant as the rest of them are on the window.

For the cleaning performance, there are studies about the contact force for the cleaning devices [21,24,25]. To clean the window perfectly, the contact force should be constant. For the better cleaning performance, the cleaning module should maintain the constant distance from the window.

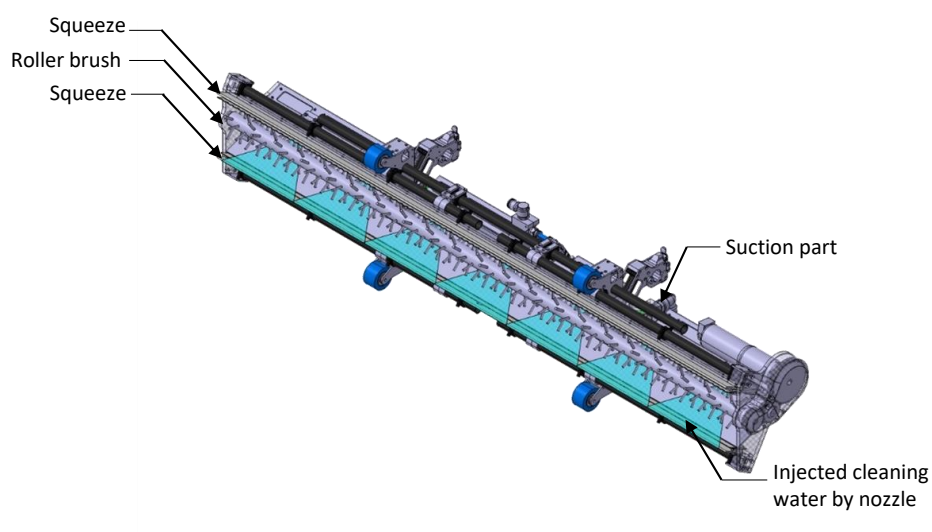

Fig. 2 Cleaning module for wall-cleaning manipulator robot

2.3 Motion and constraints of the gondola motion

To obtain a simple design, we have to investigate the motion and constraints of the gondola in the 63-story building. The basic motion of a gondola is a single-DOF, in upward and downward direction, hanging on steel wire. By the basic motion, the manipulator does not require the DOF in the vertical direction as this motion can be generated by the gondola. A lateral directional movement parallel to the glass surface is also not required for the manipulator because the lateral movement does not affect the cleaning performance. We conclude that, for the translation, a single-DOF in perpendicular direction to the glass surface is the required DOF for the manipulator.

For the orientation DOF, we have to consider the special features of the gondola in the 63-story building: an upward structure to constrain the tilting motion and a guide-rail system. Figure 3 shows the tilt motion constraints and the guide rail equipped between the glass panel and the gondola. The tilt-constraint structure is on the top and bottom of the gondola, as shown in Fig. 3(b). By the mechanical stopping mechanism, the tilting motion θa can be constrained by $-4°$ to $4°$. Particularly, the gondola in the 63-story building has a guide-rail system, as shown in Fig. 3(c). The guide-rail and gondola are connected by a 2-DOF five-bar mechanism, as exhibited in Fig. 3(c), to control the distance and orientation. From the information, we determined that the most important DOF that the manipulator should have is the yawing rotation, while the rolling DOF is constrained by the guide-rail system, and the pitching DOF is constrained by the mechanical structure. Note that a small deviation in the pitching direction does not affect the cleaning performance significantly, and it is going to be compensated by using a compliant structure design in the cleaning robot.

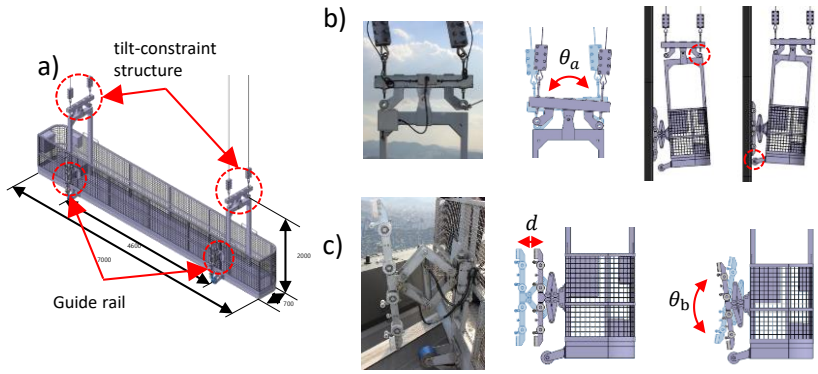

Fig. 3 Motions and constraints of the gondola in a 63-story building. a) The overall gondola, b) the mechanism over the gondola to constrain the tilting motion, and c) the guide rail mechanism to control the distance between the wall and the gondola and to constrain the orientation of the gondola.

3. 2-DOF manipulator for cleaning operation

3.1 Kinematic configuration and modeling

The wall-cleaning manipulator robot needs 2-DOF motion: translation perpendicular to the wall and yawing rotation. One DOF is the linear degree of freedom to reach the wall surface and the other DOF is the transverse rotation of the wall surface for cleaning a large area. We have determined the parallel mechanism as the mechanism of the wall-cleaning parallel manipulator. The wall-cleaning parallel manipulator is equipped with a long cleaning module to clean a large area, and thus, the payload to be mounted on the end effector is large. In order to clean a wide and large area, the accuracy of rotation of the wall in the horizontal direction is also important. As cleaning module contains long squeeze, it is important to maintain a constant force on the whole edge of the squeeze while contacted. Otherwise, water skid mark remains on the window. Therefore, manipulator's yawing has to be needed

to maintain the constant force. Because of the characteristics of the wall-cleaning parallel manipulator, it can be said that a parallel mechanism that can mount a high payload on the end-effector by mounting the actuator on the base side and has good rotation accuracy is suitable.

Figure 4 shows the 2-DOF parallel manipulator consisting of 3 prismatic joints and 5 revolute joints. Only the two prismatic joints in the base are active joints and they are driven by the actuator. The active prismatic joints were selected because the manipulator needs higher reaction rate than speed for cleaning the outer wall. These two active prismatic joints are connected to two base moving platforms, and the manipulator has two links and an end-effector where the cleaning module is mounted. The link is connected to the base by a linear guide and a rotation joint. This joint is a passive joint and is driven by a prismatic joint of the base. In the middle of the two links there is a constraint link consisting of a prismatic joint and a rotation joint that restrain the end effector. As the constraint link constrains the end effector, the manipulator has two-DOF.

According to Grübler's formula, the structure is comprised of 6 bodies, 8 joints (3 prismatic (P) joints with 1-DOF each and 5 revolute (R) joints with 1-DOF each), and thus, its mobility is $3(6-1-7)+3\cdot 1+5\cdot 1=2$; therefore, this manipulator has 2-DOF, and thus, the actuation of the 2 P-joints.

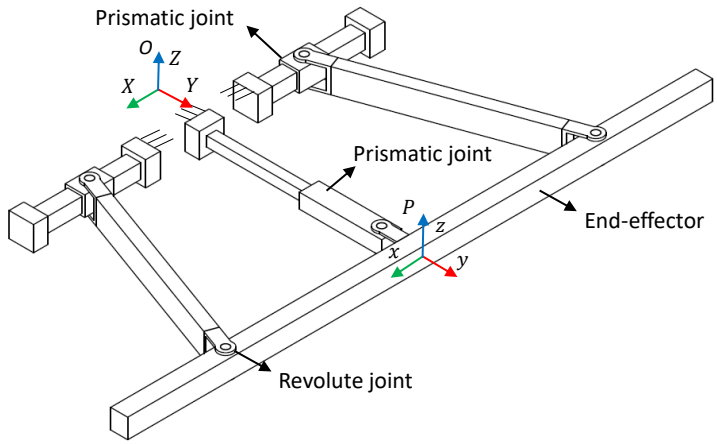

Fig. 4 Kinematic configuration of the proposed 2-DOF parallel manipulator

Figure 5 presents a simplified version of the schematic diagram of the mechanism in Fig. 4. A reference frame O-XY is fixed to the center of the base. q_1, q_2 is the distance traveled by the motor from w_1. l is the length of the link connecting the end-effector to the base moving platform and b is the distance from the center of the end-effector to the link. q_1 and q_2 are the values of the O-XY on the linear guide, and thus, the movement input vector can be written as

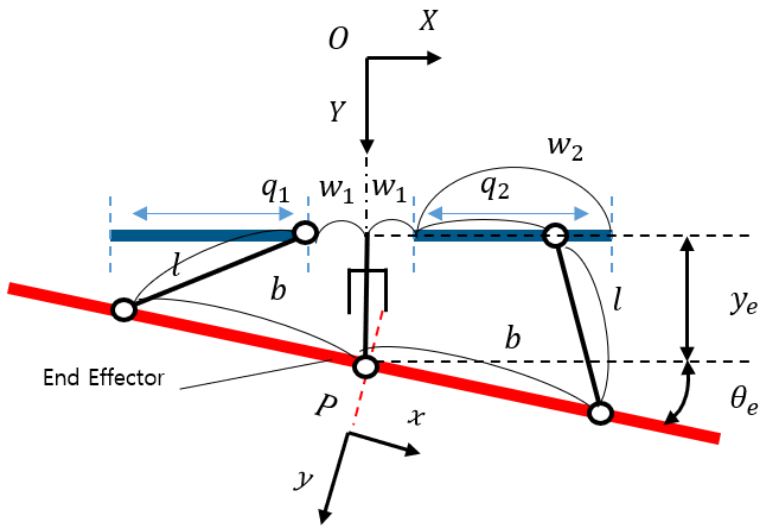

Fig. 5 Configuration diagram of the parallel manipulator.

$$\boldsymbol{q} = [q_1 \ \ q_2]^T, \tag{1}$$

and the end-effector output position vector can be written as

$$\boldsymbol{p_e} = [y_e \ \ \theta_e]^T. \tag{2}$$

The constraint equation associated with the two kinematic chains can be written as

$$(b\cos\theta_e - q_1)^2 + (y_e - b\sin\theta_e)^2 = l^2, \tag{3}$$

$$(b\cos\theta_e - q_2)^2 + (y_e + b\sin\theta_e)^2 = l^2. \tag{4}$$

The inverse kinematic problem can be written as

$$q_1 = \pm \left(b\cos\theta_e - \sqrt{l^2 - (y_e - b\sin\theta_e)^2} \right), \tag{5}$$

$$q_2 = \pm \left(b\cos\theta_e - \sqrt{l^2 + (y_e - b\sin\theta_e)^2} \right). \tag{6}$$

The equation derived above is an inverse kinematic solution of q_1 , q_2 on the location of the end effector of our mechanism. As the length of each link cannot be selected as "–" the solution can be uniquely determined by selecting "+" from "±."

3.2 Jacobian matrix

The velocity equation can be obtained by differentiating the kinematic constraint relations (3) and (4) with respect to time. It can be derived from the following equation,

$$J_q \, \dot{\boldsymbol{q}} = J_{\boldsymbol{p_e}} \dot{\boldsymbol{p}}_{\boldsymbol{e}} \, . \tag{7}$$

(1) and (2) are obtained by differentiating $\dot{\boldsymbol{q}} = [\dot{q}_1 \;\; \dot{q}_2]^T$ expressing the input velocity vector, and $\dot{\boldsymbol{p}}_{\boldsymbol{e}} = [\dot{y}_e \;\; \dot{\theta}_e]^T$ is the output velocity vector. J_q ,J_x is a 2×2 matrix that can be expressed as

$$J_{p_e} = \begin{bmatrix} y_e - b\sin\theta_e & bq_1\sin\theta_e - by_e\cos\theta_e \\ y_e + b\sin\theta_e & bq_2\sin\theta_e + by_e\cos\theta_e \end{bmatrix}, \tag{8}$$

$$J_q = \begin{bmatrix} b\cos\theta_e - q_1 & 0 \\ 0 & b\cos\theta_e - q_2 \end{bmatrix}. \tag{9}$$

Thus, the Jacobian matrix of our mechanism is

$$J = J_q{}^{-1} J_{p_e}. \tag{10}$$

3.3 Dynamic analysis

The kinematics of the 2-DOF parallel mechanism has been analyzed, and in this section we perform a dynamics analysis. The wall-cleaning parallel manipulator for the gondola must clean by pushing a large area with a constant force during the cleaning work, and thus, control must be applied in order to make constant the force applied to the left and right sides. Therefore, a dynamic analysis is essential because the dynamic part of the 2-DOF parallel mechanism manipulator should be included in the optimization.

The dynamics of the 2-DOF parallel mechanism manipulator were derived from the position and time equation according to the joint angle in the joint space [19]

$$\boldsymbol{\tau} = M(\boldsymbol{q})\ddot{\boldsymbol{q}} + V(\dot{\boldsymbol{q}}, \boldsymbol{q}) + G(\boldsymbol{q}), \tag{11}$$

$$\boldsymbol{F} = M_P(\boldsymbol{q})\ddot{\boldsymbol{p}}_{\boldsymbol{e}} + V_P(\dot{\boldsymbol{q}}, \boldsymbol{q}) + G_P(\boldsymbol{q}), \tag{12}$$

where (11) is the dynamics general form in the joint space, and (12) is the dynamics general form in the workspace. τ is the force of the actuator, $M(\boldsymbol{q})$ is the mass matrix in the joint space, $V(\dot{\boldsymbol{q}}, \boldsymbol{q})$ is the joint space velocity term, and $G(\boldsymbol{q})$ is the gravitational term in the joint space. $\boldsymbol{F}$ is a force–torque vector acting on the end-effector of the manipulator, and $\boldsymbol{p_e}$ is an appropriate work space vector representing the position and orientation of the end-effector. In addition, $M_P(\boldsymbol{q})$ is

the mass matrix on the workspace, $V_P(\dot{\boldsymbol{q}}, \boldsymbol{q})$ is the velocity term on the workspace, and $G_P(\boldsymbol{q})$ is the gravitational term on the workspace as follows:

$$\boldsymbol{\tau} = J^T \boldsymbol{F}, \tag{13}$$

$$\dot{\boldsymbol{p}}_{\boldsymbol{e}} = J\dot{\boldsymbol{q}}. \tag{14}$$

The relation of τ, the force of the actuator in the joint space, and the force–torque vector in the work space, can be derived from the relationship (13). The Jacobian relation of the joint space and work is (14), and the dynamics relation of the joint and work spaces can be derived by summarizing equations (11), (12), (13), and (14).

$$\boldsymbol{F} = J^{-T} M(\boldsymbol{q}) J^{-1} \ddot{\boldsymbol{p}}_{\boldsymbol{e}} - J^{-T} M(\boldsymbol{q}) J^{-1} \dot{J}\dot{\boldsymbol{q}} + J^{-T} V(\dot{\boldsymbol{q}}, \boldsymbol{q}) + J^{-T} G(\boldsymbol{q}). \tag{15}$$

In (15), the Coriolis terms and the centrifugal terms corresponding to the velocity terms are ignored because the operation of the manipulator is slow, and the gravity component is ignored because the contact is made by contacting the outer wall. The dynamic relationship between joint space and work space is summarized as

$$\boldsymbol{F} = J^{-T} M(\boldsymbol{q}) J^{-1} \ddot{\boldsymbol{p}}_{\boldsymbol{e}}. \tag{16}$$

3.4 Mass matrix of the manipulator

In order to analyze the dynamics of the 2-DOF parallel manipulator of the wall-cleaning parallel manipulator , the mass and inertia of link 1 and link 2 (Fig. 5), which are connected to the end-effector, and the mass and inertia of the end effector should also be considered as

$$M_P(\boldsymbol{q}) = J^{-T} M(\boldsymbol{q}) J^{-1}, \tag{17}$$

According to (16), the inertia matrix can be divided into (17). However, we must also consider mass and inertia in each link, and therefore, we need to add it to Eq. (17).

$$M_P(\boldsymbol{q}) = M_e(\boldsymbol{q}) + \sum_{i}^{2} J_i^T M_i J_{i,} \tag{18}$$

$$M_i = \begin{bmatrix} m_i & 0 \\ 0 & I_i \end{bmatrix}, \qquad M_e = \begin{bmatrix} m_e & 0 \\ 0 & I_e \end{bmatrix}. \tag{19}$$

$M_P(\boldsymbol{q})$ is the final mass matrix containing both the mass and the inertia of the link. J_i is the Jacobian matrix on the workspace at link i, which is the function of length l. $M_i(\boldsymbol{q})$ is the mass matrix of each link, and m_i and I_i are the mass and inertia components of each link. And $M_e(\boldsymbol{q})$ is the mass matrix of the end-effector and m_e and I_e are the mass and inertia components of the end-effector. Finally, the relationship between the force on the workspace and the force of the actuator can be summarized as follows:

$$\boldsymbol{F} = M_P(\boldsymbol{q}) \ddot{\boldsymbol{p}}_{\boldsymbol{e}}. \tag{20}$$

4. Optimal design

4.1 Dynamic manipulability isotropy index

The gondola-mounted wall-cleaning parallel manipulator must be mounted on a gondola and then contacted with a wide range of outer walls with constant force; thus, it is also important to optimize the manipulator in terms of control. The dynamic manipulability isotropy including the weight of the end-effector and link and the mass matrix component including the inertia component was selected as an index, and optimization was performed.

Dynamic manipulability isotropy is one of the most important indexes for evaluating the performance of parallel mechanisms [20,21]. The dynamic manipulability isotropy index, which includes the mass matrix, also helps to improve control performance, owing to the nature of exterior-wall cleaning that requires contact with the outer wall with constant force. As mentioned in Section 2.2, for the better cleaning performance, the manipulator should move any direction with more similar acceleration to maintain the distance and contact force. Therefore, the dynamic manipulability isotropy is related with the cleaning performance. First, in order to summarize the relationship between the force of the actuator in Section 3 and the force on the workspace, equations (13) and (20) are summarized in terms of acceleration on the workspace.

$$\ddot{\boldsymbol{p}}_{\boldsymbol{e}} = M_P(\boldsymbol{q})^{-1} J^{-T} \boldsymbol{\tau}. \tag{21}$$

As mentioned above, the acceleration on the workspace becomes the component of the actuator force multiplied by the inverse of the mass matrix and the inverse of

the Jacobian. $M_P(\boldsymbol{q})^{-1}J^{-T}$ stands for input force vs. output force. The scalar value K_D is summarized as follows:

$$0 \leq K_D = \frac{\lambda_{min}}{\lambda_{max}} \leq 1. \tag{22}$$

λ_{max} and λ_{min}mean the maximum and minimum values of the eigenvalue in a given posture of $M_P(\boldsymbol{q})^{-1}J^{-T}$. As KD is called the dynamic manipulability isotropy index and it is local dynamic manipulability isotropy, we will call it local dynamic manipulability isotropy (LDMI) [10]. As KD is higher, the end effector can move any direction with more similar acceleration.

Furthermore, considering all the poses of the proposed goal optimization workspace in Section 4, the value of η_D is defined as global dynamic manipulability isotropy (GDMI) as follows:

$$\eta_D = \frac{\int_w K_D \, dW}{\int_w dW}. \tag{23}$$

Here, GDMI η_D is the average of all dynamic manipulability isotropy in the targeted optimization workspace and is appropriate for the index we are going to look at.

4.2 Workspace constraints

We refer to the mechanism of the 2-DOF wall-cleaning manipulator suggested in reference [15]. In that 2-DOF wall-cleaning manipulator, the driving part is mounted on the end-effector and the dynamic load is high. We designed the manipulator with improved performance by reducing the dynamic load by bringing the actuator with the heavy actuator to the base. For the angular rotation degrees of −4° to +4° for the building outer wall in Fig. 6, we will correspond to the end-effector part as a passive rotation joint. Because of the relative angle between the exterior wall and the gondola, the length of the exterior wall and the gondola was reflected in the workspace.

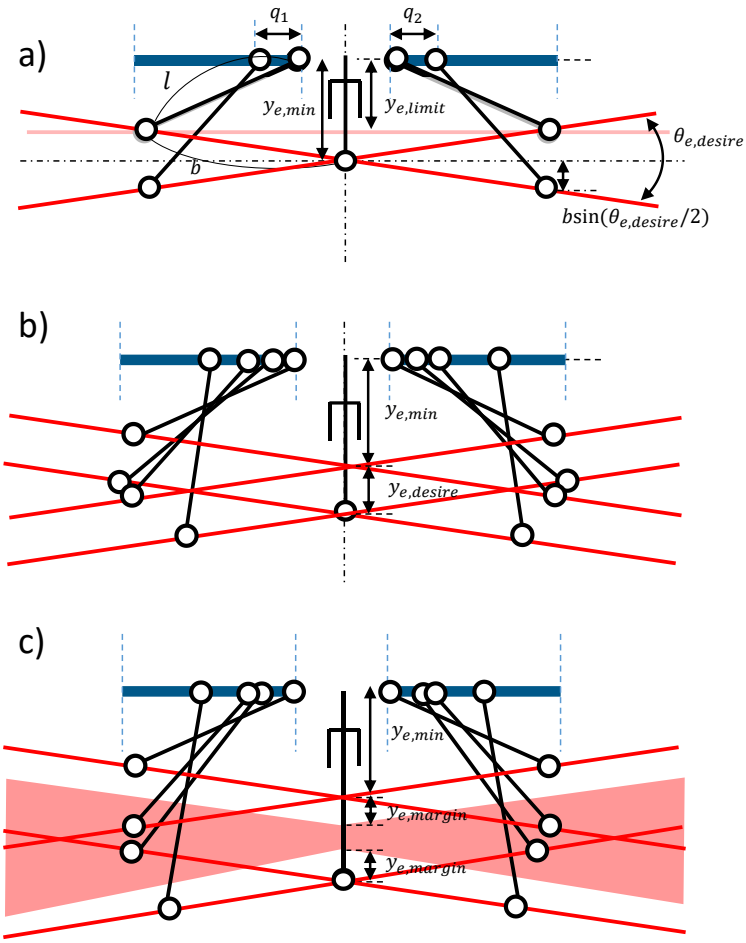

Fig. 6 Constraints on the workspace for the optimal design. a) In case of satisfying $\theta_{e,desire}$ in the minimum contraction situation, b) if $\theta_{e,desire}$ is satisfied when $\theta_{e,desire}$ is moved, and c) workspace that satisfies $\theta_{e,desire}$. The red region denotes the pre-defined workspace for cleaning operation by the end-effector denoted by the red-line.

Figure 6 shows the configuration diagram of our 2-DOF parallel mechanism manipulator. The 2-DOF parallel mechanism kinematic chain are symmetric. So variable setting is relatively simple. $y_{e,\,desire}$ is the target driving range and $\theta_{e,desire}$ is the target driving angle. $y_{e,limit}$ is the structural contraction limiting distance and $y_{e,min}$ is the minimum contraction distance considering the

workspace.

$y_{e,margin}$ is a variable given to allow a workspace to be larger than an actual driving area.

b is the link length from the center axis to the drive shaft, and $b\sin(\theta_e)$ is the drive range when it is tilted by $\theta_{e,desire}$ at the minimum contraction position by $y_{e,min}$.

Figure 6 a) shows the case of satisfying $\theta_{e,desire}$ in the minimum contraction state of the manipulator. The end-effector is reduced by $y_{e,limit}$, when q_1 and q_2 are the minimum values, and q_2 is the minimum value, when the end-effector is the clockwise rotation of $\theta_{e,desire}/2$ counterclockwise. Therefore, $y_{e,min} = y_{e,limit} + b\sin(\theta_{e,desire}/2)$.

In Fig. 6 b), $\theta_{e,desire}$ is satisfied when $y_{e,desire}$ is moved. When the end-effector moves by $y_{e,min} + y_{e,desire}$, it rotates clockwise at $\theta_{e,desire}/2$ angle. When the end-effector moves by $y_{e,min} + y_{e,desire}$, it rotates counterclockwise at $\theta_{e,desire}$/2 angle.

As can be seen in Fig. 3, there is a degree of freedom of pitch in the gondola and there are various disturbances. We set the actual driving area, $y_{e,desire}$, to 150 mm and set the red area in Fig. 6 c), which is 75 mm forward and backward from the midpoint between $y_{e,min}$ and $y_{e,margin}$, as the actual driving area.

4.3 Optimization problem definition

Optimization was performed to maximize the dynamic manipulability isotropy in order to design an optimal manipulator in the workspace selected in Section 4.2. The optimization problem is summarized in Table 1. This is the process of selecting design variables in the workspace. w_1 is the initial position of the actuator away from the center of the base. w_2 is the driving range that q_1, q_2 can move. The $q_{upperlimit}$ and $q_{loewrlimit}$ values were selected to limit the w_1 value determined by the mechanical element.

Table 1. Optimization condition

Objective function and design parameters
To find a set of design variables $\left[y_{e,min}, l, b \right]^T \in \mathbb{R}^3$ such that maximize η_D
Inequality condition
$q_i + w_2 < b\cos\frac{\theta_{e,max}}{2}\ (i = 1,2)$
$q_i + w_2 < q_{upperlimit}\ (i = 1,2)$
$q_{lowerlimit} < q_i\ (i = 1,2)$
$y_{e,min} + y_{e,desire} + y_{e,margin} < l$
Conditions 1, 2, and 3 are inequality constraints on the maximum and minimum values of q_1, q_2 and condition 4 is a constraint on the length of the link constraining the end-effector when y_e is maximized.
Equality condition
$\left(b\cos\frac{\theta_{e,max}}{2} - q_i \right)^2 + {y_{e,limit}}^2 = l^2\ (i = 1,2)$
$\left(b\cos\frac{\theta_{e,max}}{2} - q_i - w_2 \right)^2 + \left(y_{e,limit} + 2\,b\sin\frac{\theta_{e,max}}{2} + y_{e,min} \right)^2 = l^2\ (i = 1,2)$
Conditions 5 and 6 are the equality condition of the optimization variables b and l according to the movement of q_1, q_2. The relation is defined by the trigonometric function and the optimization work should be performed within the range that always satisfies the condition.

4.4. Optimal design result

Optimization was performed by using the Genetic Algorithm(GA) of MATLAB (Mathworks, 2015b). Figure 7 is the result of the optimization. Figure 7(a) shows a reconfiguration of the 2-DOF wall-cleaning manipulator in Fig. 6, which results in an optimization that satisfies the workspace. The graph of Fig. 7 (b) is λ_{max} and λ_{min} in Section 4.1 of the manipulator resulting from the optimization. As mentioned in Fig. 6, the graph shows the actual driving range of y_e within 150 mm. Fig. 7(b) is a graph showing the dynamic manipulability isotropy in an actual driving workspace. As can be seen in the graph, the dynamic manipulability isotropy decreases as y_e and θ_e become larger. It is considered that the dynamic manipulability isotropy is reduced because the inertia of the end-effector increases as y_e and θ_e increase.

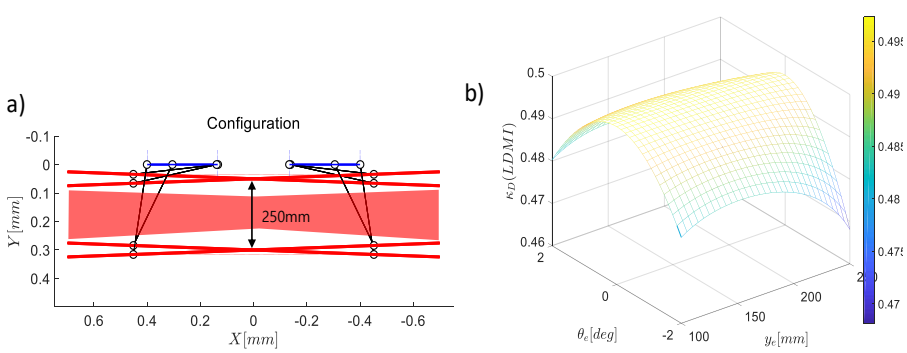

Fig. 7 Optimal design result. a) Optimal configuration and the workspace, b) dynamic manipulability isotropy according to the design parameters.

Table 2 shows the parameters of the optimized wall-cleaning 2-DOF manipulator. The values of $q_{loewrlimit}$and $q_{upperlimit}$ are the values given by the mechanical element, and $\theta_{e,max}$ is given by $\pm 2°$. The optimized w_1 and w_2 within the

satisfying workspace are calculated. $y_{e,margin}$ is the assigned value, and consequently, the optimal $y_{e,min}$, l, and b values satisfying the workspace were obtained. As a result of the optimization, GDMI was calculated as 0.4914. The wall-cleaning 2-DOF manipulator was designed by applying the optimized parameters.

Table 2. Optimized design parameters

Parameter	Value	Parameter	Value
w_1	140 mm	$y_{e,min}$	50 mm
$q_{lowerlimit}$	100 mm	$y_{e,margin}$	100 mm
$q_{upperlimit}$	400 mm	l	319.9 mm
w_2	260 mm	b	452.3 mm

Figure 8 shows the comparison of dynamic manipulability ellipsoid for the optimal GDMI results (η_D = 0.4914) with the case when GDMI is 0.4500 ($y_{e,min}$= 50 mm, l = 350.3 mm, b = 503.8 mm). The red line and the blue dotted line are the ellipsoids of the GDMI 0.4914 manipulator and the GDMI 0.4500 manipulator in task space of y_e and θ_e, respectively. It shows that the dynamic manipulability of the optimized manipulator is more isotropic than non-optimized manipulator. We are going to prove the improvement of dynamic manipulability experimentally in Section 5.

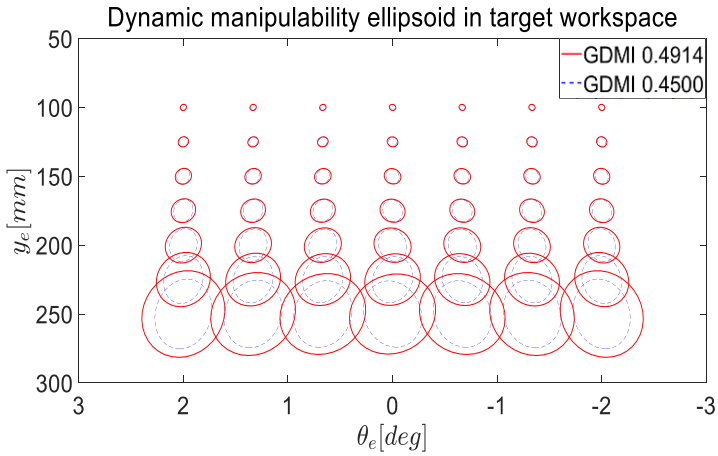

Fig. 8 Dynamic manipulability ellipsoid for y_e, θ_e in target workspace

5. Prototype and experiment

Based on the configuration and optimal design results in the previous sections, we designed and developed a working prototype. Figure 9 shows the design and the assembled prototype. The prototype is composed of three components: cleaning unit, 2-DOF manipulator, and main body, which is equipped on a gondola. In the main body, there are several components such as electronics, solution supply, and suction motors. The size of the prototype is 1400 × 500 × 650 mm3 and the weight is 81 kg.

The cleaning unit is developed for the cleaning operation. The detailed design and analysis are presented in [23]. The cleaning module is composed of a spray nozzle, brush, squeeze, and suction. The cleaning operation proceeds by spraying the solution, brushing the solution, squeezing the solution, and retrieving the solution by suction. The design parameters are optimized experimentally [23].

The 2-DOF manipulator is located between the main body and the cleaning unit. The length of the manipulator is manufactured based on the design in Section 4. The

weight of the manipulator and main body is about 63 kg. We used two geared DC motors (Maxon RE50, Power : 200 W Voltage : 48 V No load speed : 7580 rpm nominal torque : 177 mN·m) for the actuators with a ball screw (Misumi C-BSSTK1510-440-F20-P10-KC8-RLC, Precision grade : C7 lead : 5 mm shaft diameter : 10 mm shaft length : 20 mm) to generate the linear motion. The linkages are made by carbon fiber pipes.

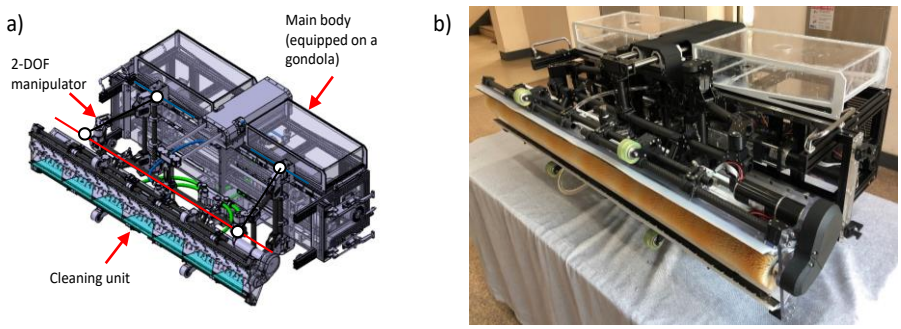

Fig. 9 a) Prototype design and b) photograph of the assembled prototype.

Figure 10 shows the workspace test of the manipulator. After adding the significant payload of the cleaning unit, the prototype successfully manipulated it in the pre-defined workspace. The manipulator can move the cleaning unit for the 2-DOF, translation perpendicular to the surface and yawing rotation.

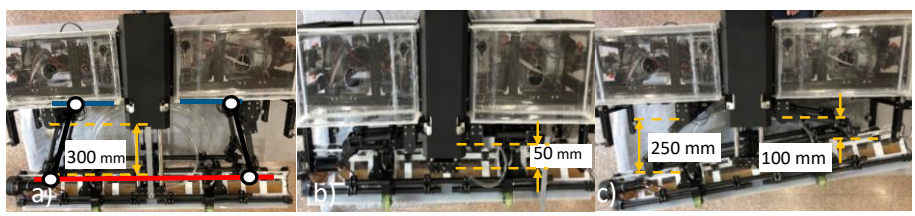

Fig. 10 Workspace test of the cleaning unit manipulated by the developed 2-DOF manipulator

We performed experiment to verify the improvement of GDMI. The GDMI defines the relation between the output motion and input force based on inertia and Jacobian matrix as shown in (21). To check the GDMI, we made linear input motion to make y_e(linear motion) be sinusoidal motion and θ_e(rotational motion) be sinusoidal, respectively. By measuring the input force of linear guide for each y_e and θ_e motion, we can determine the input force isotropy characteristics for the independent motions.

Figure 11 shows the experimental set-up to measure the input force. Two load cell sensors are equipped to measure the force of linear guide as shown in Fig. 11. We have conducted experiments to verify the dynamic manipulability isotropy of an optimized manipulator (GDMI : 0.4914, $y_{e,min}$= 50 mm , l=319.9 mm, b=452.3 mm) and a low GDMI manipulator(GDMI : 0.4500, $y_{e,min}$= 50 mm , l=350.3 mm, b=503.8 mm). We conducted two experiments with each manipulator, one is linear motion, the other is rotational motion. Linear motion input is given by sinusoidal wave (magnitude : 15 mm, frequency : 1.8 Hz) and rotational motion input is also given by sinusoidal wave(magnitude : 2 degree, frequency : 1.8 Hz)

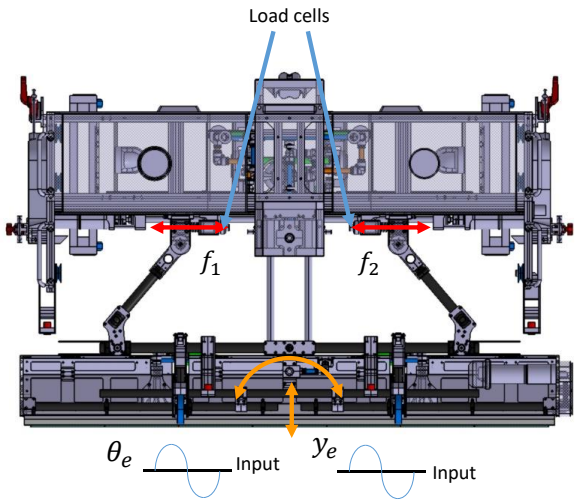

Fig. 11 Load cell sensors measure the force input by the operation of the manipulator.

In linear and rotational motion experiment, load cell sensor that mounted on manipulator base measure forces f_1 and f_2. Due to the mechanical symmetry, the magnitude of f_1 and f_2 are measured to be the same; so we used f_1 for the analysis. We defined input force isotropy(η_I) from the experiment to validate the GDMI as follows:

$$\eta_I = \frac{\int |f_{1,\theta_e}| \, dt}{\int |f_{1,y_e}| dt} \tag{24}$$

Figure 12 shows that input force ellipsoid during manipulator linear motion and rotational motion. red line ellipsoid and blue dotted line ellipsoid are the GDMI 0.4914 manipulator input force e and the GDMI 0.4500 manipulator input force, respectively. Finally, we verified that input force isotropy is more isotropic in 0.4914 GDMI manipulator than 0.4500 GDMI manipulator. Input force ellipsoid is calculated by f_1 in joint space, so ellipsoid size is inverse to ellipsoid size in Fig. 8. Higher and lower GDMI manipulator have 0.9371 and 0.8845 input force isotropy. Two manipulators have an 8.5% GDMI difference and 6% difference in isotropy.

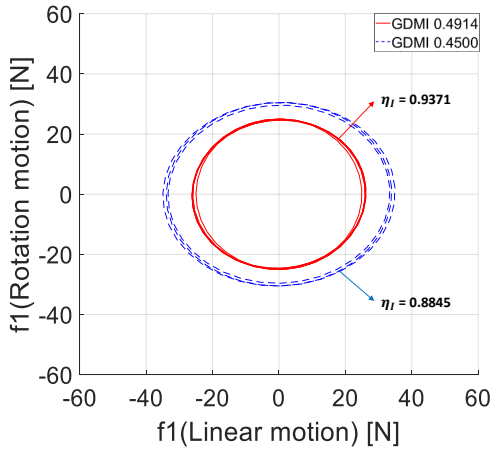

Fig. 12 Input force ellipsoid graph of optimized and non-optimized manipulator

And then, we performed the cleaning experiment on a test bench by maximum GDMI manipulator. The design of the test bench is shown in Fig. 13. The test bench consists of external frame, winch and rope to simulate the gondola movement, glass panel, and prototype. We used a geared DC winch (UDT-240T). To control the force and position of the manipulator to the glass panel, we used the impedance controller with disturbance observer developed in the previous research [22].

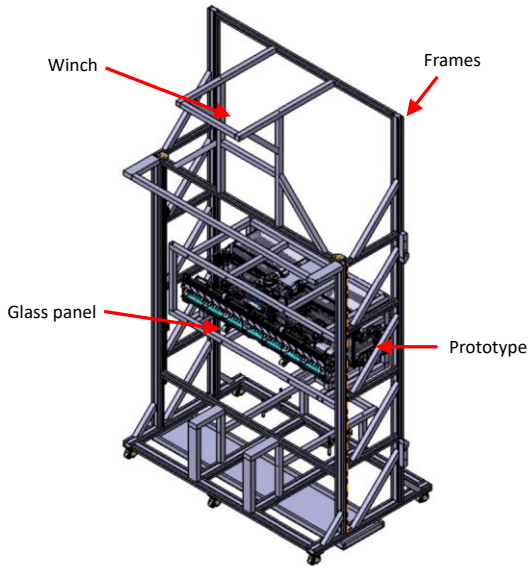

Fig. 13 Test bench for the cleaning experiment

Figure 14 shows the results of the cleaning experiment. We contaminated the glass panel with dirt and cleaned the glass panel with the prototype. As can be seen in Fig. 13, the glass surface gets clean after the cleaning device moves. For various distances and orientations, we performed the same test and obtained successful cleaning results.

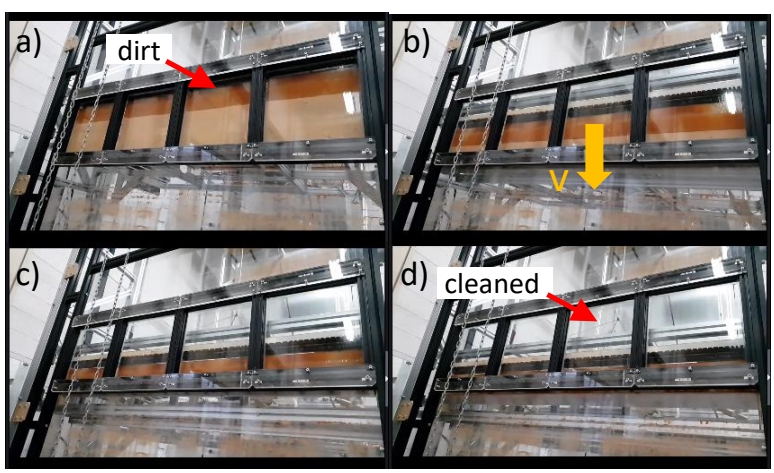

Fig. 14 Cleaning operation on a test bench and cleaning results.

6. Conclusions

This paper presented a research on the manipulator for a wall-cleaning operation, which manipulates a wide and heavy cleaning unit on a gondola. The use conditions of a 63-story building gondola were investigated, and two important-DOF, of translation and rotation, were determined. We proposed a parallel manipulator to achieve these two-DOF with a wide end-effector by using a six-bar mechanism with translational actuators and a constraint linkage in the middle. Based on the parallel mechanism, an optimal design was conducted based on kinematics and dynamics to maximize the dynamic manipulability isotropy considering the cleaning operation A prototype was built to test the performance. According to the result of the input force measurement experiment with the prototype, GDMI is enhanced. It was verified that the optimized manipulator satisfies the workspace, and cleaning performance is enhanced according to the cleaning experiment. In the near future, we are going to perform a field test in the 63-story building and the obtained knowledge will be shared.

References

[1] Skyprocy, Cyprus, http://www.skyprocy.com/ (retrieved at Jul. 4, 2018)

[2] Highrise, IPC Eagle, http://www.ipceagle.com/products/highrise (retrieved at Jul. 4, 2018)

[3] T. Akinfiev, M. Armada, S. Nabulsi, "Climbing cleaning robot for vertical surfaces," Industrial Robot: An International Journal, vol. 36, pp. 352-357, 2009.

[4] N. Elkmann, D. Kunst, T. Krueger, M. Lucke, T. Felsch, T. Sturze, "SIRIUSc – façade cleaning robot for a high-rise building in Munich, Germany," in Proc. of the 7th International Conference on Climbing and Walking Robots, Madrid, Spain, 2004, pp. 1033-1040.

[5] E. Gambao, M. Hernando, "Control System for a semi-automatic façade cleaning robot," in Procc of the 23rd ISARC, Tokyo, Japan, 2006, pp. 406-411.

[6] H. Zhang, F. Zhang, W. Wang, R. Liu, G. Zong, "A series of pneumatic glass-wall cleaning robots for high-rise buildings," Industrial Robot: An International Journal, vol. 34/2, pp. 150-160, 2007.

[7] S. Moon, J. Huh, D. Hong, S. Lee, C. Han, "Vertical motion control of building facade maintenance robot with built-in guide rail," Robotics and Computer-Integrated Manufacturing, vol. 31, pp. 11-20, 2015.

[8] Jun Wu, Guang Yu, Ying Gao, Liping Wang, " Mechatronics modeling and vibration analysis of a 2-DOF parallel manipulator in a 5-DOF hybrid machine tool," Mechanism and Machine Theory, vol. 121, pp. 430-445, 2018.

[9] Jun Wu, Ying Gao, Binbin Zhang, Liping Wang, "Workspace and dynamic performance evaluation of the parallel manipulators in a spray-painting equipment," Robotics and Computer-Integrated Manufacturing, vol. 44, pp.199-207, 2017.

[10] Jun Wu, Binbin Zhang, Liping Wang, "A Measure for Evaluation of Maximum

Acceleration of Redundant and Nonredundant Parallel Manipulators," Journal of Mechanisms and Robotics, vol. 8, pp.021001.1-021001.7

[11] Jun Wu, Jinsong Wang, Liping Wang, Tiemin Li, "Dynamics and control of a planar 3-DOF parallel manipulator with actuation redundancy," Mechanism and Machine Theory, vol.33, pp.835-849, 2009.

[12] X.-J. Liu, J. Wang, "On the optimal kinematic design of the PRRRP 2-Dof parallel mechanism," Mechanism and Machine Theory vol. 47, no. 9, pp. 1111-1130, 2006.

[13] X. Liu, L. Guan, J. Wang, "Kinematics and closed optimal design of a kind of PRRRP parallel manipulator," Journal of Mechanical Design, Transaction of the ASME, vol. 129, no. 5, pp. 558-563, 2006.

[14] H. Asada, "Dynamic analysis and design of robot manipulators using inertia ellipsoids," in Proc. IEEE International Conference on Robotics and Automation, 1984, pp. 94-102.

[15] O. Khatib, A. Bowling, "Optimization of the inertia and acceleration characteristics of manipulators," in Proc. IEEE International Conference on Robotics and Automation, 1996, pp. 2883-2889.

[16] A. Bowling, O. Khatib, "The dynamic capability equations: a new tool for analyzing robotic manipulator performance," IEEE Transactions on Robotics and Automation, vol. 21, no. 1, pp. 115-123, 2005.

[17] G. Liu, Y. Chen, Z. Xie, X. Geng, "GA/SQP optimization for the dimensional synthesis of a delta mechanism based haptic device design," Robotics and Computer-Integrated Manufacturing, vol. 51, pp. 73-84, 2018.

[18] 63-building, https://en.wikipedia.org/wiki/63_Building, (retrieved at Jul. 7, 2018).

[19] J. J.Craig, Introduction to robotics: mechanics and control, 2005, Pearson.

[20] T. Yoshikawa, “Dynamic manipulability of robot manipulators,” in Proc. IEEE International Conference on Robotics and Automation, pp. 1033-1038, 1985.

[21] Q. Hao, “GA-based dynamic s manipulability optimization of a 2-DoF planar parallel manipulator,” in Proc. IEEE Conference on Robotics, Automation and Mechatronics, pp. 46-51, 2010.

[22] T. Kim, S. Yoo, H.S. Kim, J. Kim, “Design and force-tracking impedance control of a 2-DOF wall-cleaning manipulator using disturbance observer and sliding mode control,” in Proc. IEEE International Conference on Robotics and Automation, 2018, pp. 4079-4084.

[23] J. Hong, S. Yoo, I. Joo, J. Kim, H.S. Kim, T. Seo, “Optimal parameter design of a cleaning device for vertical glass surface,” submitted for publication, 2018.

[24] Kim, T., Jeon, Y., Yoo, S., Kim, K., Kim, H., & Kim, J. “Development of a wall-climbing platform with modularized wall-cleaning units,” Automation in Construction, Vol. 83, pp. 1-18, 2017.

[25] Imaoka, N., Roh, S., Yusuke, N., & Hirose, S., “SkyScraper-I: Tethered whole windows cleaning robot,” Intelligent Robots and Systems (IROS), 2010 IEEE/RSJ International Conference on, pp. 5460-5465, 2010.

국문 초록

고층빌딩 곤돌라 탑재용 외부 유리창 청소로봇 유닛 개발

고층 빌딩의 벽은 청소 근로자가 일 년에 수 차례 직접 곤돌라에 탑승하여 청소합니다. 청소 작업은 단순 노동이지만 고층에서의 작업이므로 매우 위험합니다. 그리하여 로봇을 사용하여 이 작업을 자동화하는 지속적인 여러 가지 연구가 있었습니다. 청소 작업에 가장 중요한 청소 성능을 높이기 위해서는 청소 조건이 청소 환경에 적응해야 합니다. 본 연구에서는 외벽 청소작업에 사용할 매니퓰레이터를 설계하고 제작합니다. 고층빌딩에 유지보수와 청소작업을 위해 의무적으로 설치되어있는 곤돌라에 탑재하는 새로운 개념의 청소 로봇입니다. 한국의 고층 건물을 조사해서 나온 설계 요구 사항에서 두 가지 중요한 매니퓰레이터의 자유도 (DOF)를 결정했습니다. 그 후, 모션을 구현하기 위한 병렬 매니퓰레이터 메커니즘을 설계했습니다. 곤돌라에서 높은 청소 성능을 얻기 위해 병렬 매커니즘의 동적 인덱스를 기반으로 설계 변수를 최적화 하였습니다. 그 후, 프로토 타입을 조립하고 세척 성능을 테스트 벤치에서 확인합니다.

주요어 : 외벽 청소, 병렬 메커니즘, 최적화 디자인, 동적 모델링

학 번 : 2017-22895